Original Article

Institution of MECHANICAL ENGINEERS

Journal of AEROSPACE ENGINEERING

Proc IMechE Part G:
J Aerospace Engineering
0(0) 1–15

DOI: 10.1177/0954410018813432
journals.sagepub.com/home/pig

SAGE

Effects of orifice divergence on hollow cone spray at low injection pressures

Kushal Ghate and Thirumalachari Sundararajan

Abstract

In this work, the effects of orifice divergence on spray characteristics have been reported. Parameters such as spray cone angle, liquid sheet thickness, coefficient of discharge, break-up length, and Sauter mean diameter are greatly affected by the half divergence angle (θ_D) at orifice exit. An experimental investigation is carried out in which water sprays from five atomizers having half divergence angle values of 0°, 5°, 10°, 15°, and 20° are studied at different injection pressures. Image processing techniques are used to measure spray cone angle and break-up length from spray images, whereas the sheet thickness outside the orifice exit is obtained using the scattered light from a thin Nd-YAG Laser beam. Phase Doppler interferometry is also used to obtain the Sauter mean diameter at different axial locations. A few numerical simulations based on the volume of fluid method are included to obtain physical insight of the liquid film development and air core flow inside the atomizer. It is observed that the liquid sheet thickness as well as tangential and radial components of velocity at orifice exit are modified drastically with a change in half divergence angle. As a consequence, the droplet size distribution is also altered by variation in the nozzle divergence angle. The mechanism responsible for such variations in the spray behavior is identified as the formation of an air core or air cone inside the liquid injector as a result of the swirl imparted to the liquid flow.

Keywords

Orifice divergence, liquid sheet thickness, phase Doppler interferometry, volume of fluid, spray atomization, air core formation

Date received: 7 August 2018; accepted: 23 October 2018

Introduction

The pressure swirl atomizer (simplex atomizer) is one of the simplest fuel injectors, which is widely used in liquid rocket engines, aircraft engines, boilers, etc. because of its good atomization quality and relative ease of manufacture. In a simplex atomizer, a swirl chamber followed by a circular orifice, generates a thin liquid sheet with swirling motion (Figure 1(a)). Multiple tangential ports are provided to impart swirling motion to the fuel, which spreads out in the form of a hollow cone sheet, because of the centrifugal force acting on it. Due to interfacial instabilities, the conical liquid sheet subsequently breaks down to form droplets. The air from the surrounding enters into the atomizer because of the low-pressure region created by the swirling liquid sheet near the axis, forming an air core within the liquid jet. The air core interacts with the liquid sheet and influences the coefficient of discharge and other important spray characteristics. A schematic diagram of the simplex atomizer is shown in Figure 1(a). The internal geometry of the atomizer plays a major role in guiding the liquid film flow as well as the reverse air core flow, in the vicinity of the orifice exit. In turn, spray parameters such as the liquid sheet thickness, break-up length, and droplet size distribution are influenced significantly. In the present study, the effect of orifice divergence angle on important spray parameters is investigated experimentally and computationally. While the experimental investigation highlights the effects of orifice geometry on the spray parameters, the computational analysis provides explanations for the observed trends.

Department of Mechanical Engineering, Indian Institute of Technology Madras, Chennai, India

Corresponding author:
Thirumalachari Sundararajan, Department of Mechanical Engineering, Indian Institute of Technology Madras, Chennai 600036, Tamil Nadu, India.
Email: tsundar@iitm.ac.in

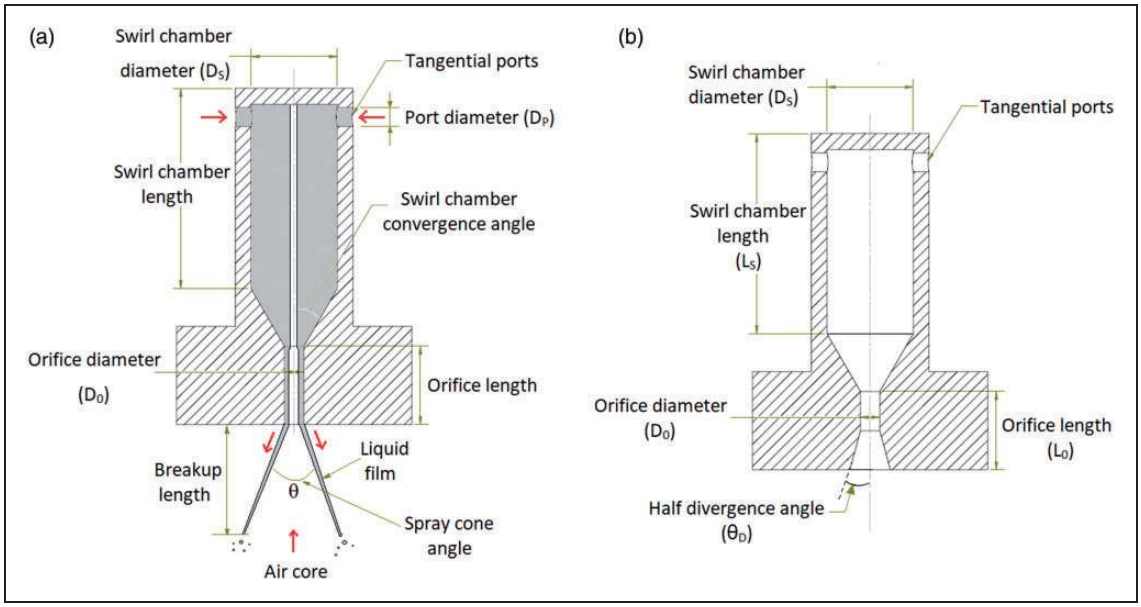

Figure 1. Simplex atomizer: (a) schematic diagram of a conventional atomizer; (b) injector geometry with divergent portion.

It is evident that the liquid properties, injection flow conditions, and the atomizer geometry govern the performance of an atomizer.[1] The spray cone angle is one of the most important performance parameters of a high-pressure swirl atomizer, which influences spray dispersal. The spray cone angle (θ) is determined as

$$\theta = 2 \times \tan^{-1}\left(\frac{\bar{W}}{\bar{U}}\right) \tag{1}$$

where $\bar{W}$ and $\bar{U}$ represent the average swirl and axial velocity components respectively, at the orifice exit. The Sauter mean diameter (SMD) of the spray, which is important from the point of view of droplet evaporation and combustion, is defined as

$$SMD = \frac{\Sigma N_i D_i^3}{\Sigma N_i D_i^2} \tag{2}$$

where N_i represents the number of droplets and D_i represents the mean diameter of droplets in the i^{th} diameter range. Other important parameters of a liquid spray, which are of prime interest, are the liquid sheet break-up length and the coefficient of discharge.

Several researchers have studied various performance aspects of spray atomizers. Vijay et al.[2] presented a review of the research work on the performance of a simplex atomizer. The paper comprehensively discusses the different regimes of operation and the important results obtained from various studies. Ballester and Dopazo[3] compared the performance of 20 different nozzle geometries. New empirical correlations were proposed for the variations of discharge coefficient and spray cone angle. The influence of viscosity was observed to be large in the spray cone angle correlations for small-scale as well as large-scale simplex atomizers.

Chu et al.[4] performed an experimental investigation on flat plate and cylindrical type pressure swirl atomizers and validated the data with the analytical results available in the literature. The effects of parameters such as orifice diameter and liquid injection pressure on spray were comprehensively studied. Lee et al.[5] characterized the flow in a pressure swirl atomizer for various fuel temperatures and injection pressures. For low temperature applications, higher injection pressure values were recommended to ensure good fuel atomization and dispersal. Durdina et al.[6] presented a novel design of pressure swirl atomizer with spill line and compared its performance with those of conventional pressure swirl atomizers. Particle image velocimetry (PIV) and phase Doppler anemometry (PDA) were used to get the velocity distribution and droplet sizes at different locations.

The flow inside a pressure-swirl atomizer often involves multi-phase interactions, due to the presence of an air core surrounded by a thin liquid sheet. These interactions are highly dependent on the internal geometry of the atomizer and the liquid swirl momentum. Landwehr et al.[7] introduced a new visualization technique to track the surface waves in the hollow cone liquid film. Good agreement was observed with the results obtained by a fiber-sensor-based frequency analysis. Fu et al.[8] used an electrical conductance method to measure the liquid film thickness in an open-end swirl injector. The proposed method can be used not only in the steady condition but also in the pulsating condition. Fu et al.[9] analyzed spray characteristics of a unique open-end swirl injector, which has no convergent angle. New empirical

equations were proposed as discrepancies were observed between the experimental data and the results obtained by empirical equations derived for closed-end injectors (with convergent angle). Kim et al.[10] investigated the mixing and atomization characteristics of liquid–liquid coaxial swirl injectors by modifying the recess length between the inner and outer injectors. Mixing efficiencies were found to be higher by about 10% for internal mixing injection as compared to that of external mixing injection. The liquid film flowing inside the orifice is typically measured using a conductance probe, which is an intrusive method. Kim et al.[11] measured the liquid film thickness at orifice exit by the electrical conductance method and proposed an improved relation by incorporating the orifice length effect in an existing analytical equation. Schubring et al.[12] used the planar laser-induced fluorescence method for direct visualization of the liquid film and its thickness measurement. Kang et al.[13] experimentally studied the effects of sleeve geometry on combustor ignition performance. For higher sleeve divergence angle, greater spray cone angle and smaller SMD were observed. Radke et al.[14] investigated the performance of a double swirl coaxial injector using liquid oxygen and liquid fuel for different recess orifice diameters, by controlling the divergence angle at the orifice exit. X-ray radiography was used to measure the sheet thickness and break-up length, for different recess orifice diameters.

Halder et al.[15] experimentally investigated the influence of simplex atomizer geometry on the size of air core. It was observed that as swirl chamber convergence angle increases, the air core diameter marginally increases inside the swirl chamber. The swirling liquid sheet emanating from the orifice imparts rotary motion to the air core, which in turn, gives rise to a low-pressure region near the axis. To understand the effects of air flow and pressure variations on the spray development of direct injection gasoline engines, several injectors have been studied at different operating conditions by Moon et al.[16] Xue et al.[17] studied the effects of different geometric ratios involving the diameters of the inlet slot, swirl chamber, and exit orifice, as well as the lengths of swirl chamber and exit orifice, on liquid film thickness, spray cone angle, and discharge coefficient. Ma[18] carried out a detailed study of the flow field in the swirl chamber of a large scale simplex atomizer using laser Doppler velocimetry (LDV) and particle image velocimetry (PIV). It was observed that the flow field inside the simplex atomizer is axisymmetric even for an atomizer with only two inlet tangential ports. Muthuselvan et al.[19] have recently discussed the effects of injector geometry (tangential port area) on important spray characteristics such as the cone angle, discharge coefficient, and mean drop size.

Von Lavante and Maatje[20] numerically investigated the performance of pressure swirl atomizers using different flow solvers. After comparing the predicted results with experimental data, axisymmetric simulations were recommended as economical and effective by the authors. Datta and Som[21] theoretically predicted air core diameter, coefficient of discharge, and spray cone angle in pressure swirl atomizers. Yeh[22] established a numerical model to study the flow in plain orifice atomizers with chamfered or rounded orifice inlets. It was concluded that an atomizer with a rounded orifice inlet is beneficial for better atomization. Nouri-Borujerdi and Kebriaee[23] have developed an axisymmetric, laminar/turbulent two-phase flow solver to simulate the flow in pressure swirl atomizers. The level set equation was explicitly used for determining the liquid–gas interface. Amini[24] performed a theoretical analysis using the integral momentum method to investigate the boundary layer flow inside the pressure swirl atomizer. It was concluded that the internal flow structure plays a very important role in determining the nozzle performance.

Xue et al.[25] numerically investigated the influence of various internal geometrical parameters of the simplex atomizer including nozzle divergence angle at the exit. It was found that the spray cone angle increases if the half divergence angle increases in the range 10°–40°. On the other hand, Liu et al.[26] considered half divergence angle ranging from 0° to 10° for their numerical and experimental studies. Here, spray cone angle was found to be decreasing with increase in half divergence angle. Musemic and Walzel[27] employed a nozzle with trumpet shaped exit and experimentally analyzed the atomization performance. It was observed that the film emanating out of the simplex atomizer follows the trumpet contour due to the Coanda effect.

The studies available in the literature show a strong dependence of spray characteristics on the atomizer geometry. Any change in the atomizer geometry, which leads to finer atomization and wider dispersal of spray will be an important development. The velocity components at the orifice exit greatly affect the spray cone angle and spray dispersion. In particular, the tangential and radial components of velocity aid spray dispersion in the lateral direction. Therefore, a proper control of liquid velocity and sheet thickness at the orifice exit is required to achieve good atomization and spray dispersion. In the present work, the effect of an extended divergent portion of the spray nozzle for guiding hollow cone spray development is investigated, at different injection pressures. In particular, the development of air core near the nozzle exit and its interaction with the liquid sheet up to the location of primary breakup, are studied both numerically and experimentally. The effects of nozzle divergence on all the important parameters such as spray cone angle, liquid sheet thickness, break-up length, discharge coefficient, and average droplet size variation, are described in detail.

Methodology

Experimental methodology

Five atomizers with different half divergence angle (θ_D) values of 0°, 5°, 10°, 15°, and 20° are used, keeping all other internal atomizer dimensions constant. The geometric details of the simplex atomizer with divergent portion are shown in Figure 1(b) and the corresponding dimensions are tabulated in Table 1. Except for the half divergence angle at the exit, all other parameters are same for all the orifices. Water is used as the working fluid for generating the spray and it is injected into an open test section through a simplex atomizer with the help of compressed air. The injection pressure (ΔP) is varied from 1 to 7 bar (gage) and the corresponding water mass flow rate ranges from 0.3 to 1.5 L/min. A pressure gage having the least count of 0.05 bar is installed upstream of the injector to monitor the actual injection pressure. The error in liquid mass flow rate is estimated as ±0.05 L/min.

Spray imaging. Figure 2 shows the schematic of experimental setup, consisting of the atomizer, rotameter, pressure regulator, camera, backlighting, and the diffuser plate. To capture images of the transient spray, a high-speed PCO Dimax HS1 camera is utilized. Spray is visualized at the rate of 6000 frames per second, with an exposure time of 10 µs and image size of 1 megapixel per frame. Backlighting and diffuser plate are also used to provide proper illumination during the experiments. The spray cone angle and break-up length are obtained from the images, at different operating conditions.

Sheet thickness measurement. The imaging system used to capture the hollow cone sheet comprises a low-speed camera, a narrow Laser beam and a convex lens. A schematic of the experimental setup and the optics is shown in Figure 3. A double-pulsed Nd:YAG laser is used for illumination purpose. Only the first pulse of the dual-pulsed laser is used for visualizing the liquid sheet. The convex lens is employed to converge the laser beam to obtain a narrow beam diameter (40 µm) at the focal point. A PCO Pixelfly USB camera is synchronized with the laser pulse and is used for imaging at a spatial resolution of 1392 × 1040 pixels. A field of view (FOV) with 15 mm × 11 mm size is selected for visualizing the liquid sheet. The liquid sheet with a velocity of about 20 m/s will leave the FOV in approximately 0.55 ms. To capture instantaneous images, a pulse width of 5 ns and exposure time of 20 µs have been set for the laser beam and camera, respectively. Images are acquired inside a dark enclosure with no other lights, except the laser beam. The laser and camera are placed perpendicular to each other for gathering the scattered light from the liquid sheet. The laser beam is passed via the convex lens and is focused at the spray axis. The laser beam is traversed downwards in steps of 3 mm (FOV-1 and FOV-2) to capture the variation of liquid sheet thickness in axial direction, before the sheet breaks up into ligaments or droplets. Camera is focused at the point where the beam intersects the liquid sheet.

The approximate width of FOV is about 15 mm, which corresponds to 1392 pixels. This implies that the smallest resolvable length-scale (1 pixel) is approximately 11 microns. A total of 300 images were captured for each flow condition. After discarding a few over or under-illuminated images, the remaining well-illuminated images are processed using MATLAB. The following steps are carried out during the post-processing of images:

(i) Cropping the image to focus on the locations where unbroken liquid sheet is present.
(ii) Removal of noise generated because of scattering of light by foreign particles or fine recirculating droplets.
(iii) Averaging of images (Figure 4).

Table 1. Geometric details of simplex atomizer.

Geometric parameter	Atomizers				
	D1	D2	D3	D4	D5
half divergence angle (deg)	0	5	10	15	20
Orifice diameter (mm)	1 (same for all atomizers)				
Orifice length (mm)	4 (same for all atomizers)				
Swirl chamber diameter (mm)	4.4 (same for all atomizers)				
Swirl chamber length (mm)	9 (same for all atomizers)				
Tangential port diameter (mm)	0.8 (same for all atomizers)				
Number of tangential ports	3 (same for all atomizers)				

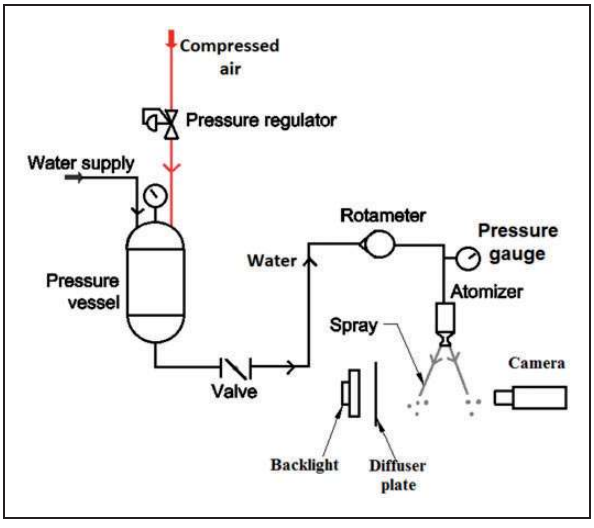

Figure 2. Schematic view of experimental setup for spray imaging.

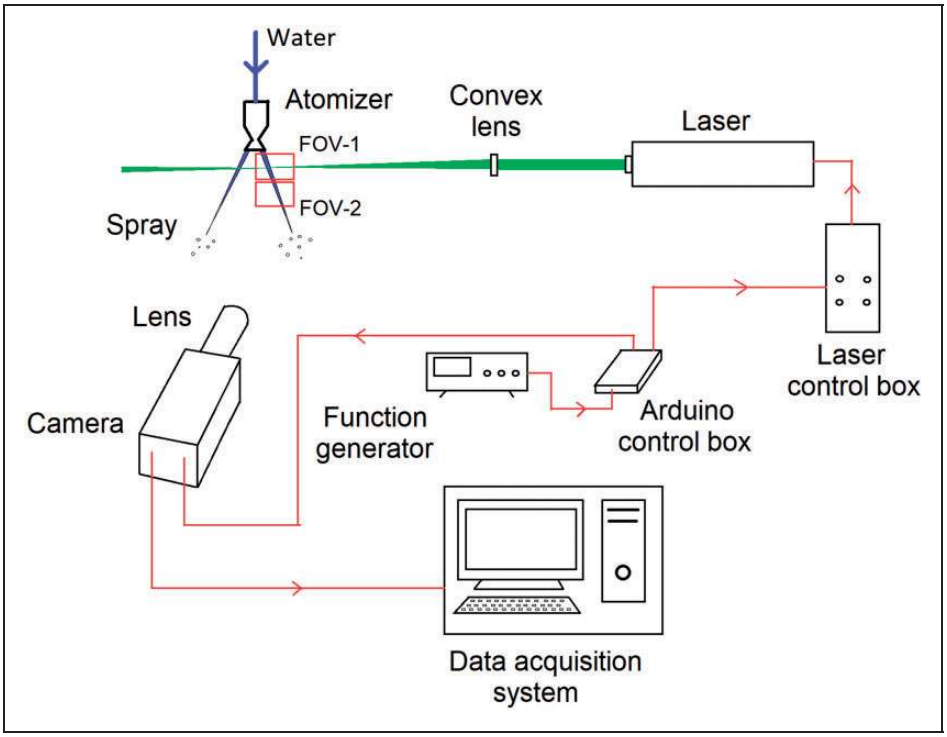

Figure 3. Schematic diagram of experimental setup for sheet thickness measurement.

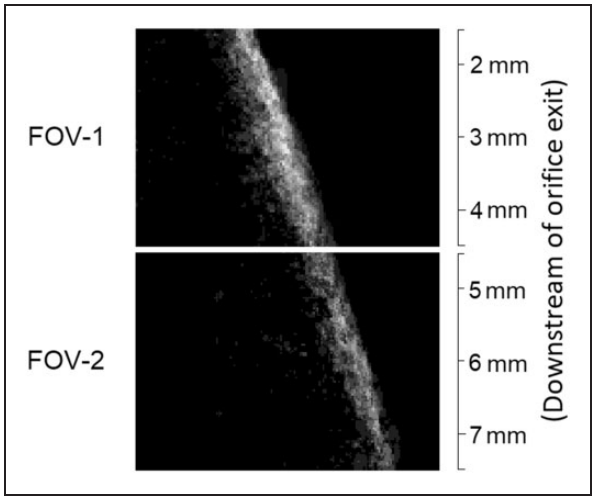

Figure 4. Averaged image of FOV-1 and FOV-2.

(iv) Plotting of pixel intensity variation across the liquid film at different axial locations downstream of the orifice exit (Figure 5).
(v) Conversion of pixel dimension into length (in millimeters) to get sheet thickness value. Since the averaged image represents the superposition of hundreds of instantaneous images, the intensity profiles (Figure 5) show substantial variation across the film. This intensity variation is employed to evaluate the average film thickness at each axial location. A threshold value of minimum intensity = 0.1 × maximum intensity is used to identify the edge of the film for evaluating film thickness, as shown in Figure 5.

It is to be borne in mind that the liquid film flow undergoes dynamic variations rapidly. Thus, when hundreds of instantaneous liquid sheet images are superimposed, the brighter (high intensity) zones correspond to locations where liquid film is present most of the time. The low intensity zones correspond to locations where liquid film or ligaments are present occasionally. Thus, trimming zones of low intensity (less than 10% of maximum intensity) provides a reasonable estimate of the average sheet thickness at the particular location. In the plots of Figure 5, the 10% intensity cut-off line for identifying the film edges is also included for reference. The experimentally obtained sheet thickness values are also compared with the values obtained from volume of fluid (VOF) simulations.

Phase Doppler interferometry. A phase Doppler interferometer (Artium PDI) is used to measure the drop size distribution at different radial locations, for axial sections at 90 mm, 120 mm, and 150 mm downstream of the orifice exit and injection pressures of 5 bar and 7 bar. The PDI has two solid-state lasers (of 473 nm and 532 nm wavelength) which intersect each other to form a probe volume. The phase difference between the reference beam and the light scattered by the droplets is recorded by the receiver and used to calculate the droplet diameter. SMD values at different radial locations are compiled and averaged to get mean SMD values at the particular axial plane. The axial locations of 90 mm, 120 mm, and 150 mm have been selected so that light scattering occurs due to

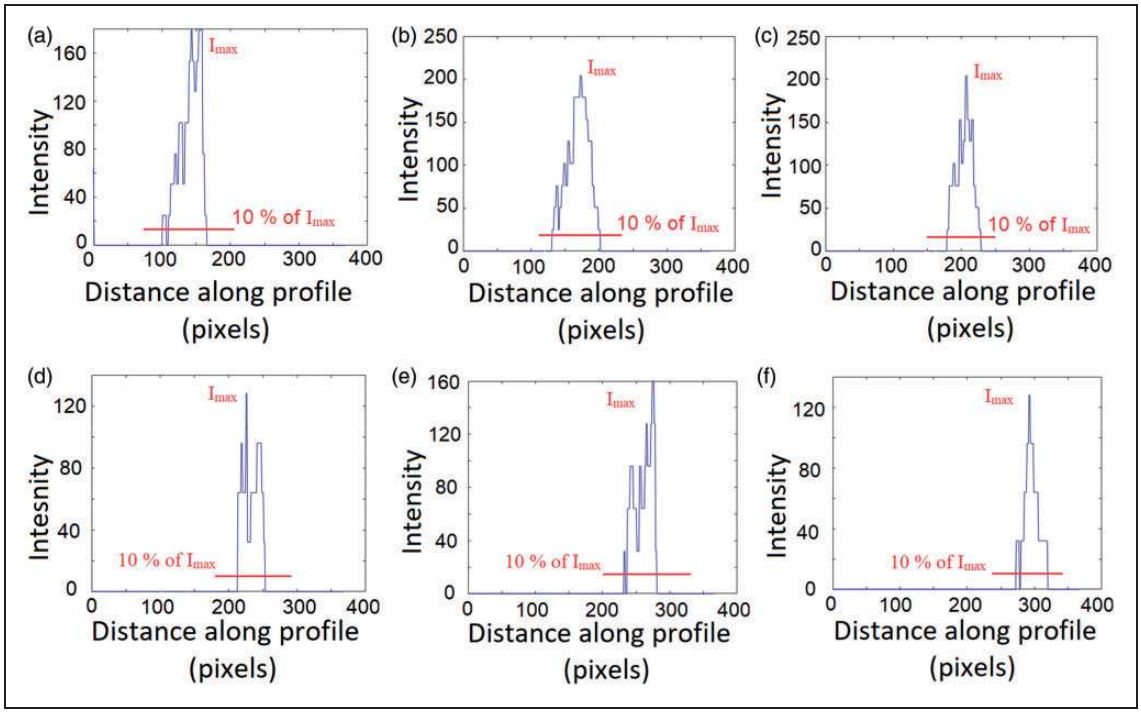

Figure 5. Intensity profiles at different axial locations of FOV-1 and FOV-2: (a) at 2 mm; (b) at 3 mm; (c) at 4 mm; (d) at 5 mm; (e) at 6 mm; (f) at 7 mm.

droplets only and not because of ligaments produced during spray break-up.

Numerical methodology

A computational study is also performed to obtain some physical insight about the flow inside the simplex atomizer and its evolution just outside the orifice. The two-phase flow comprising liquid and air streams within the swirl chamber, is modelled to analyze phenomena such as air core formation and liquid sheet development. A fixed-grid methodology based on VOF technique is used. The incompressible Navier–Stokes equations are solved by the finite volume approach using ANSYS Fluent 16.1. A single set of governing equations is shared by the constituent fluids (water and air) and the volume fraction variation of each fluid is tracked in all the computational cells. For tracking the sharp interface position between the fluids, a geometric reconstruction scheme generalized from the work of Youngs and David[28] is used, based on piecewise linear representation of the interface. The piecewise linear interface calculation (PLIC) algorithm approximates the local interface shape by straight line (or plane) segments normal to the gradient of volume fraction in each computational cell. Three steps are involved in the interface reconstruction scheme namely, tracing a linear interface in a partially filled cell, calculating the advecting amount of fluid through each face, and calculating the updated volume fraction in each cell using the flux balance for each time step. The effect of surface tension is included in the simulations using the continuum surface force (CSF) approach. The VOF simulations are carried out only until the location where liquid stream remains continuous i.e. before the primary break-up.

The pressure-implicit with splitting of operators (PISO) algorithm by Issa[29] is used for solving the pressure-velocity linked equation while momentum, Reynolds stresses and all other flow parameters are discretized using the second-order scheme to achieve higher accuracy in modelling. PREssure STaggering Option (PRESTO) spatial discretization scheme is used for pressure correction equation, in view of the steep pressure gradients present in swirling flows. The Reynolds stress model (RSM) is used to incorporate turbulence effects as it is known to be accurate for swirling flows. RSM closes the Reynolds-averaged Navier–Stokes equations by solving transport equations for the Reynolds stresses, together with an equation for the dissipation rate.

An equivalent axisymmetric flow is assumed inside the simplex atomizer and the tangential ports are replaced with an equivalent annular inlet. The width of the annular inlet (W) is calculated by equating the total area of tangential ports with that of the equivalent axisymmetric inlet. Thus

$$W \times \pi D_S = N_P \times A_P = N_P \times \frac{\pi D_P^2}{4} \tag{3}$$

where D_S is the swirl chamber diameter, D_P, A_P, and N_P are the tangential port diameter, tangential port

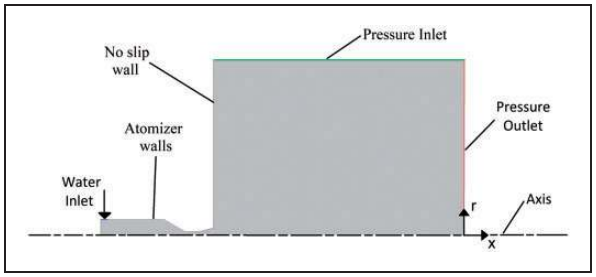

Figure 6. Axisymmetric geometry employed for the computational study.

area, and the number of ports, respectively. The tangential and radial velocity components at the inlet (W_{inlet}, V_{inlet}) are calculated based on the angular momentum and the kinetic energy of the liquid at the tangential inlet ports, using the following equations

$$W_{inlet} = \frac{Q}{N_P \times A_P} \times \left(\frac{D_S - D_P}{D_S}\right) \tag{4}$$

$$V_{inlet} = \left[\left(\frac{Q}{N_P \times A_P}\right)^2 - W_{inlet}^2\right]^{\frac{1}{2}} \tag{5}$$

where Q is the volumetric flow rate.

The velocity components are prescribed at the annular inlet whereas a constant pressure condition is prescribed on the external side boundaries of the air region to simulate air entrainment, as shown in Figure 6. The pressure outlet condition is specified at the outlet of the computational domain, with pressure value equal to zero gauge pressure. No-slip stationary wall condition is applied at the wall boundary. For air and water respectively, the viscosities are specified as 1.7894×10^{-5} and 1.003×10^{-3} kg/m−s and the densities are 1.225 and 998.2 kg/m^3, respectively. The surface tension at the interface is specified as 0.072 N/m.

The continuous movement of air inside the simplex atomizer forming an air core often makes the liquid flow unsteady. Thus, all the results predicted by the numerical analysis are at quasi-steady condition when the spray development is nearly complete and the cone angle, break-up length and velocity components of the liquid sheet do not vary much with time. Therefore, time-averaged quantities are used for comparison purposes.

Grid Independence study. The VOF results are sensitive to the grid size. Therefore, it is important to perform grid independence study to obtain results which are not dependent on mesh size. For this purpose, three different grid sizes are used in the simulations. The spray cone angle θ is calculated for the three grids and compared with experimental results as shown in Table 2. Experimental and numerical results corresponding to five different atomizers (D1, D2, D3, D4, and D5) and an injection pressure of 3 bar, are used for comparison.

Table 2. Comparison of spray cone angle calculated by experimental and numerical approaches.

Atomizers	Grid I θ (deg)	Grid II θ (deg)	Grid III θ (deg)	Experiments θ (deg)
D1	17.17	20.46	20.50	21.24
D2	18.57	23.71	23.82	24.67
D3	20.31	27.20	27.38	27.81
D4	20.31	27.51	28.01	28.39
D5	24.64	32.02	32.11	32.57

For atomizer D1, grid I contains 249,710 cells (average grid size: 63 μm), grid II contains 589,589 cells (average grid size: 41 μm), and grid III contains 1,264,157 cells (average grid size: 28 μm). Maximum error is 26.96%, 3.89%, and 3.48% for grids I, II, and III, respectively, with respect to the experimental data. Furthermore, the results predicted for grids II and III are very close to each other and hence, grid II is used for all further simulations to reduce the overall simulation cost.

Results and discussion

Measurement of spray cone angle

Spray cone angle is one of the most important spray characteristics, which governs the extent of spray dispersal within the combustion chamber. Instantaneous spray images are captured using high speed camera for different atomizers at injection pressures ranging from 1 bar to 7 bar. Figures 7 and 8 represent the processed instantaneous spray images for atomizers D1, D3, and D5 at an injection pressure of 1 bar and 7 bar, respectively.

In the case of cone angle, a set of 100 images is first averaged and processed with the help of Matlab and ImageJ software to get the time-averaged values. Figure 9 shows the numerically predicted spray configuration at an instant when the spray is nearly steady. Several images showing volume fraction contours of water and air at different time instants are processed to obtain the spray cone angle values from computational results. The experimental range of spray cone angle values are plotted for different atomizers and different injection pressures in Figure 10. The numerically predicted average spray cone angle values are also plotted in the same graph for comparison. Good agreement is observed between the experimental and numerical values, with a maximum deviation of ±6.5%.

Three different regimes are observed in Figure 10 for the spray cone angle variation with divergence angle, at different injection pressures. In regimes I and III, the spray cone angle is found to be increasing with increase in θ_D, whereas in regime II spray cone angle decreases with increase in divergence angle. At higher pressures, the variation of spray cone angle at

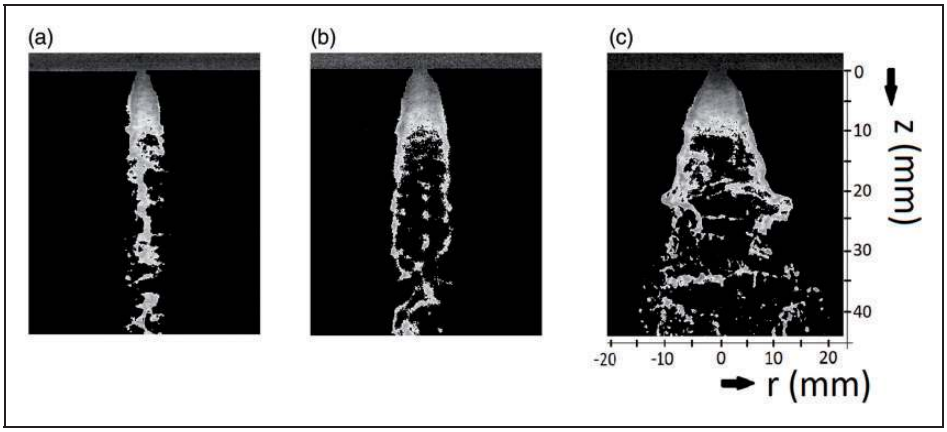

Figure 7. Processed instantaneous experimental images of spray for different atomizers at an injection pressure of 1 bar. (a) Atomizer D1. (b) Atomizer D3. (c) Atomizer D5.

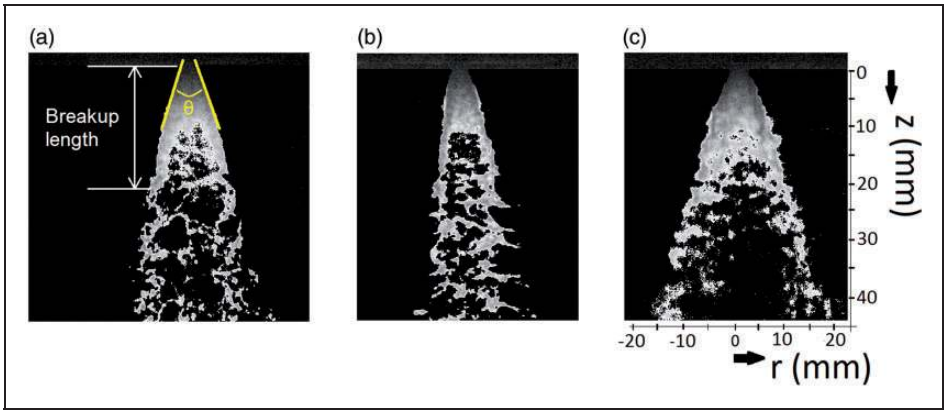

Figure 8. Processed instantaneous experimental images of spray for different atomizers at an injection pressure of 7 bar. (a) Atomizer D1. (b) Atomizer D3. (c) Atomizer D5.

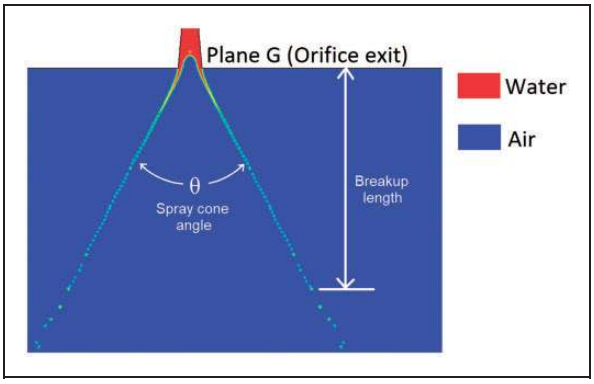

Figure 9. Measurement of spray cone angle and break-up length by computational analysis for atomizer D2 at a time instant of 15 ms.

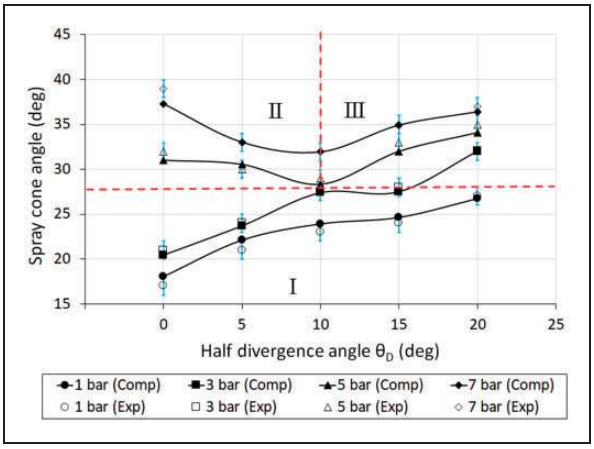

Figure 10. Spray cone angles for different atomizers at different injection pressures (comp – computational; exp – experimental).

lower divergence angles fairly matches with the trends observed by Liu et al.[26] For higher divergence angles, the present data match with the trends observed by Xue et al.[25] The main difference noted between atomizers with lower divergence angle and higher divergence angle is the extent to which spray cone angle changes with the change in injection pressure. For instance, experimental spray cone angle for atomizer D1 ($\theta_D = 0^\circ$) changes from 17° to 39° (approximately 130%), whereas for atomizer D5 ($\theta_D = 20^\circ$), it changes from 28° to 42.5° (approximately 53%) with an increase in injection pressure from 1 bar to 7 bar. Clearly, atomizer D5 with higher divergence angle is found to be less sensitive to change in injection

pressure as compared to other atomizers having lower divergence angle. The trends observed in Figure 10 are explained using the computational results presented in the next section.

Computational results

Formation of air core is very helpful as air movement inside as well as outside the atomizer gives rise to instability near the liquid–air interface. Air core is basically a consequence of low-pressure region created near the axis because of the swirling liquid in an injector. Figure 11 shows the temporal evolution of liquid flow within the atomizer D3 (half divergence angle: 10°). Tangentially introduced liquid flow adheres close to the wall during liquid filling and eventually the liquid stream forms a thin film in the throat and divergent portion. The unfilled portion close to the axis leads to air core formation. Larger air core forces thinner liquid sheet to emanate from orifice, subsequently giving rise to smaller drop sizes, after liquid sheet break-up.

In some cases, air does not penetrate throughout the atomizer to form an air core. Instead, an air cone is formed in the vicinity of the orifice exit. In either case, a high velocity air stream is observed, which moves into the orifice and returns back close to the liquid sheet. Figure 12 shows the fully developed air cone and streamlines of air stream.

At low pressures, in general, a closed tulip structure is observed for the liquid film.[19] This structure opens up as divergence angle increases. The widening of orifice mouth at higher divergence angle, helps in guiding the liquid flow outwards from the spray axis. Thus, in regime I, spray cone angle monotonically increases as divergence angle increases (Figure 10). At higher pressure (5 bar and 7 bar) and larger divergence angle, orifice exit admits entry of atmospheric air into the atomizer body for the formation of air cone or air core.

The velocity vectors for atomizer D2 (regime II) and atomizer D5 (regime III) corresponding to 5 bar condition, are plotted in Figure 13 to illustrate reverse flow of air into the atomizer. High air velocity value (~36 m/s) is observed at the center of orifice exit for the latter case. The high-velocity air flow aids in the dispersal of liquid flow in the outward direction while moving out of the atomizer in its return path. This phenomenon of high-velocity air core flow aiding liquid flow dispersal outwards is dominant for higher divergence angle and higher pressure range. Further, the average air core velocity values at different planes upstream of the orifice exit for different atomizers are plotted in Figure 14(b). Maximum variation is observed for the atomizer D5 (half divergence angle: 20°). This can be attributed to the shape of the orifice divergence, which accelerates the air moving upstream of the orifice. The strong reverse air flow pushes the liquid sheet outwards during its return path, resulting in larger cone angle values. These

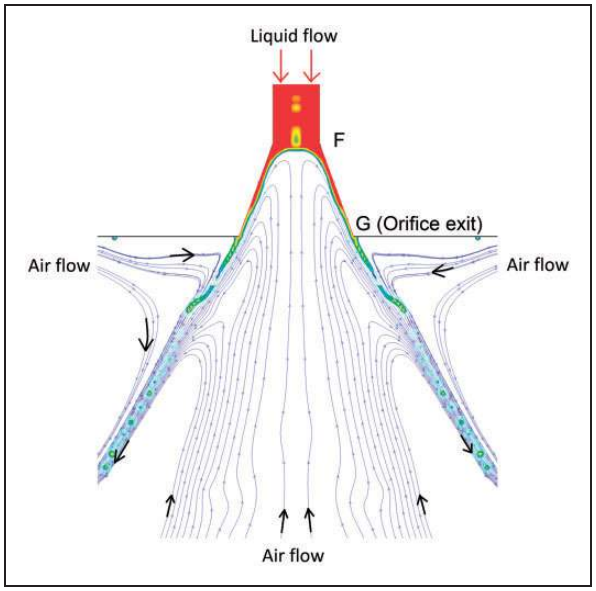

Figure 12. Computationally predicted streamlines of air flow for atomizer D4 ($P_{inj} = 1$ bar).

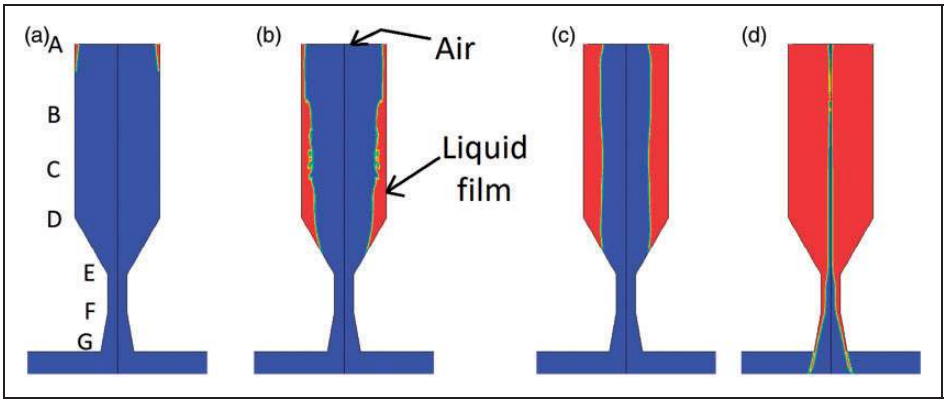

Figure 11. Formation of the air core inside the atomizer D3: (a) 0.15 ms; (b) 2.8 ms; (c) 5.3 ms; (d) 8.35 ms.

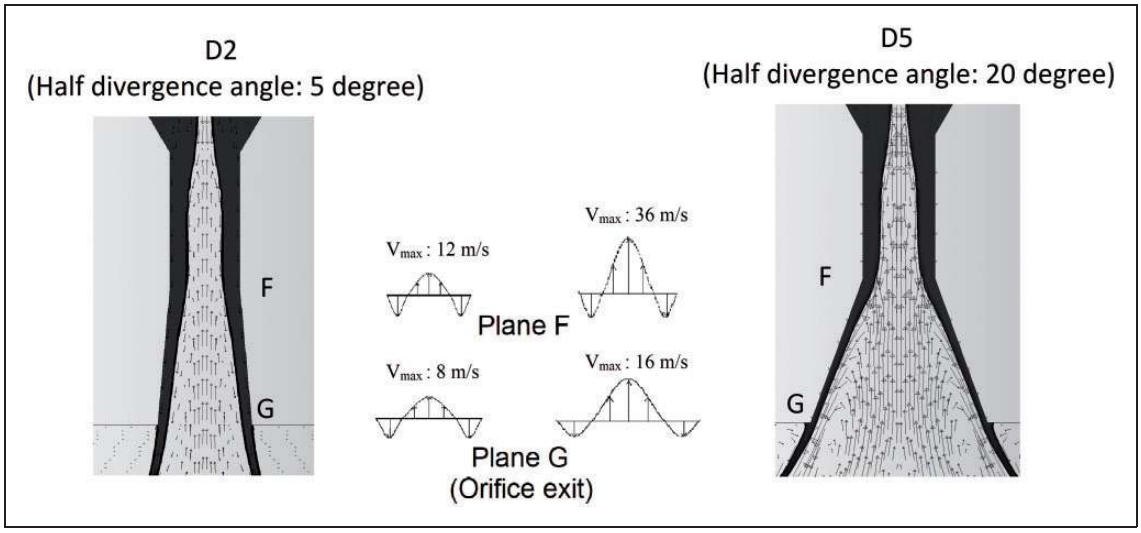

Figure 13. Movement of air stream near orifice for different half divergence angle by computational analysis.

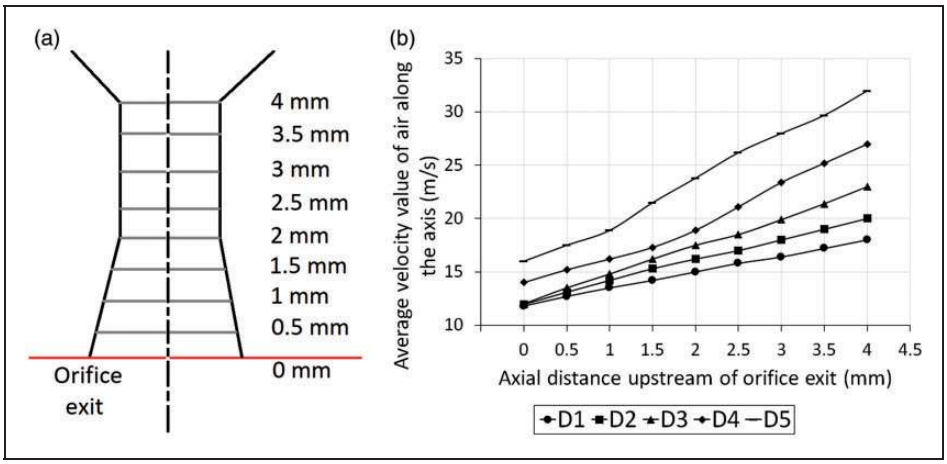

Figure 14. Numerically predicted variation of average air core velocity upstream of orifice exit: (a) planes across the orifice length; (b) air core velocity at different planes.

two-phase flow aspects lead to spray cone angle increase with an increase in the divergence angle, in regime III.

The normalized velocity components calculated from numerical analysis for different atomizers at an injection pressure of 5 bar have been plotted in Figure 15. The axial and tangential velocity components are minimum and maximum respectively for atomizer D3 (half divergence angle: 10°), which gives rise to the lowest value of spray cone angle observed in Figure 10, at higher injection pressures.

For a given orifice geometry, as injection pressure is increased, spray opens up and forms an air core inside the atomizer. Providing a large divergence angle at the orifice exit is an effective way of forcefully forming an air core. Figure 16 shows the extent of air entrainment inside the simplex atomizer predicted for different atomizers at a fixed injection pressure of

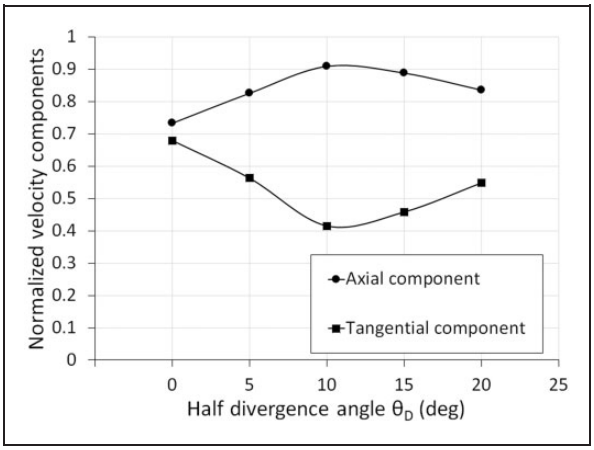

Figure 15. Computed variation of normalized velocity components at orifice exit for different atomizers at an injection pressure of 5 bar.

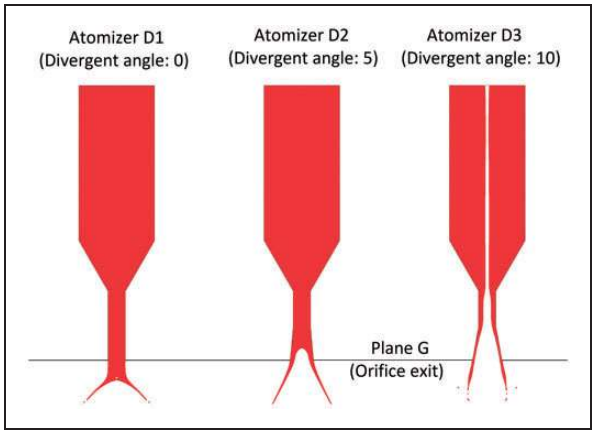

Figure 16. Predicted instantaneous spray images for different nozzle divergence angles at 5 bar injection pressure.

Table 3. Computationally predicted trends of air core/air cone formation.

Injection pressure	Atomizers				
	D1	D2	D3	D4	D5
1 bar	–	–	Air cone	Air cone	Air core
3 bar	–	Air cone	Air cone	Air core	Air core
5 bar	–	Air cone	Air core	Air core	Air core
7 bar	Air cone	Air core	Air core	Air core	Air core

5 bar. Atomizer D1 exhibits no air entrainment inside the atomizer, whereas atomizer D2 shows air cone formation in the vicinity of the orifice. Atomizer D3 with higher divergence angle shows the formation of a fully developed air core throughout the atomizer. Air core ensures the formation of thin sheet at orifice exit, which ultimately leads to finer atomization. Table 3 shows the conditions (atomizer and injection pressure) at which air cone or air core or no air entrainment inside the atomizer is observed in quasi-steady state. In the cases where air core is formed, the instantaneous interfacial shape (between the liquid and air) is generally not cylindrical but found to be wavy in nature.

At higher injection pressure (5 bar), it is observed (Figure 16) that spray cone angle decreases with θ_D when air stream starts penetrating inside the atomizer (atomizers D1, D2, D3) corresponding to regime II in Figure 10. When the air stream penetrates completely inside the atomizer and forms a fully developed air core, spray cone angle increases with further increase in θ_D (atomizers D3, D4, D5).

Coefficient of discharge and sheet thickness

Table 4 shows the actual volumetric flow rates measured for different atomizers and injection pressures.

Table 4. Experimentally measured variation of actual flow rate (L/min) with injection pressure.

Injection pressure	Atomizers				
	D1	D2	D3	D4	D5
1 bar	0.58	0.51	0.51	0.52	0.54
3 bar	0.99	0.85	0.82	0.83	0.82
5 bar	1.22	1.18	1.17	1.17	1.18
7 bar	1.40	1.33	1.29	1.31	1.33

Coefficient of discharge (C_D) is defined as the ratio of actual flow rate through the atomizer to the theoretical mass flow rate, given by the expression

$$C_D = \frac{\dot{m}_a}{\rho_l A_0 \left(\frac{2\Delta P}{\rho_l}\right)^{\frac{1}{2}}} = \frac{\text{Actual flow rate}}{\text{Ideal flow rate}} \tag{6}$$

where ρ_l is the liquid density and A_0 is the orifice area.

The experimental data for C_D are evaluated for all the cases corresponding to five different atomizers and four different injection pressures (1 bar, 3 bar, 5 bar, and 7 bar). Ideal flow rate is proportional to the square root of static pressure drop across the atomizer for a given atomizer geometry. In the simulations, average static pressure at plane A (inlet of swirl chamber) and plane G (orifice exit) are employed for the calculations of ideal flow rate, whereas a pressure gage is used to measure injection pressure in experiments. The actual flow rate is measured using a rotameter in the experiments with a least count of 0.05 L/min. The same flow rate value is used in the computational analysis also. Coefficient of discharge (C_D) values determined from experimental and computational analyses are plotted in Figure 17. It has been shown by Chu et al.[4] that for a given injector geometry (i.e. orifice diameter), C_D is more or less constant at different injection pressures. In the present experiments also, same trend is observed for C_D with a maximum deviation of 9% (Figure 17). As the divergence angle changes, the exit diameter of the orifice changes. In such a case, spray parameters vary because of the change in divergence angle as well as a change in exit orifice diameter. It is observed that C_D decreases monotonously with increase in the divergence angle. The area covered by the liquid sheet at the orifice exit governs the actual mass flow rate of liquid through the atomizer. Liquid sheet thickness (t) is normalized with orifice throat radius (r_t) and the normalized sheet thickness ($t^* = t/r_t$) for different experimental and computational cases is plotted in Figure 18. With the increase in injection pressure, the spray opens up from tulip geometry to a fully developed hollow cone spray. In the case of a tulip-shaped spray, the liquid sheet occupies the complete area of the orifice. In such cases, normalized sheet thickness reaches its maximum value. In the case of a hollow cone spray, an

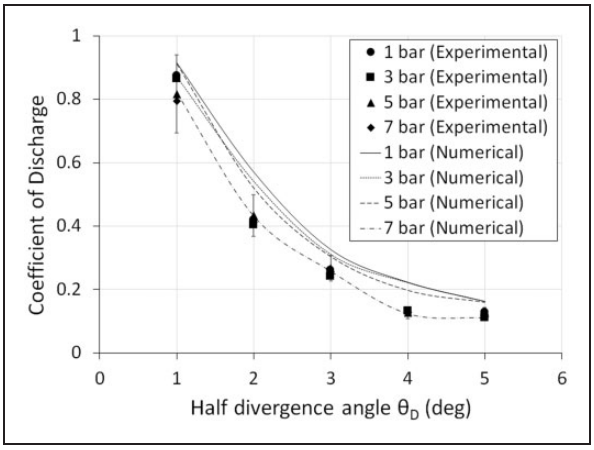

Figure 17. Experimental and numerical variation in coefficient of discharge with half divergence angle.

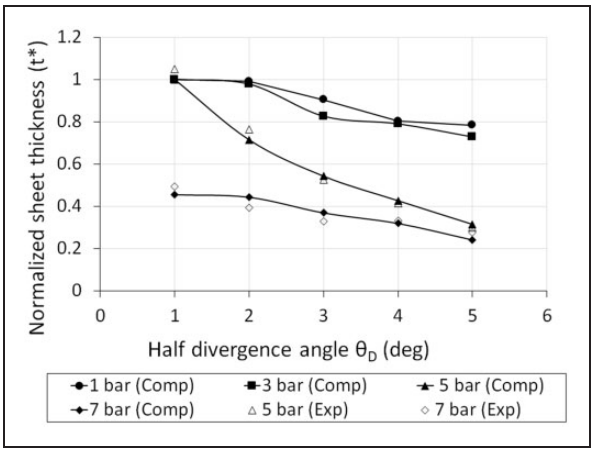

Figure 18. Variation of normalized sheet thickness for different atomizers at injection pressures of 1 bar, 3 bar, 5 bar, and 7 bar (comp – computational; exp – experimental).

air cone or air core is formed which blocks a portion of the orifice exit area, thereby reducing the normalized liquid sheet thickness value (t^*).

This trend of normalized sheet thickness decreasing with increase in θ_D corroborates with the observed variation of C_D. From Figures 17 and 18, it is confirmed that sheet thickness at the orifice exit and coefficient of discharge of the atomizer are inter-related. At a fixed injection pressure, both the quantities show decreasing trend with increase in θ_D. For a fixed orifice divergence (particular injector geometry), sheet thickness reduces with increase in injection pressure; still C_D remains almost constant because of the change in the velocity components across the liquid sheet at orifice exit, which counteracts the change in flow area of liquid stream. Sheet thickness at a particular location inside the atomizer is governed by the size of air core at that location. The sheet thickness values at different axial planes of the five different atomizers are plotted in Figure 19 at an injection pressure of 5 bar. In Figure 19, the section E-F corresponds to the constant area throat portion and F-G represents the divergent

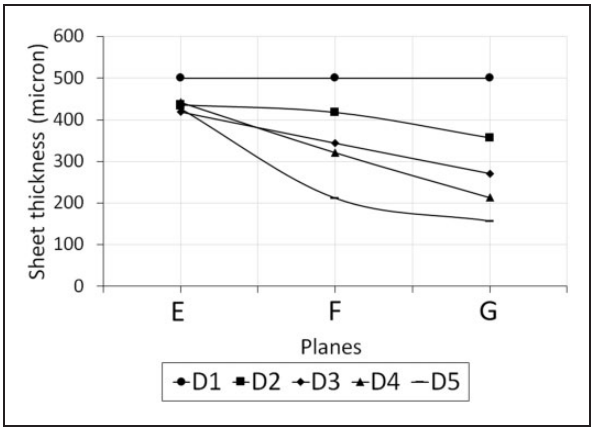

Figure 19. Variation of sheet thickness inside the atomizer for different atomizers at injection pressures of 5 bar.

Table 5. Sheet thickness (mm) by analytical equation[30] and experiments.

	t (mm), analytical		*t* (mm), experimental	
Atomizers	5 bar	7 bar	5 bar	7 bar
D1	0.309	0.284	0.500	0.227
D2	0.290	0.267	0.357	0.221
D3	0.289	0.266	0.271	0.184
D4	0.266	0.244	0.213	0.159
D5	0.240	0.220	0.157	0.120

portion towards the exit (refer to Figure 11(a)). An abrupt decrease in the sheet thickness value is observed for atomizer D5 as compared to other atomizers, implying a sharp increase in the air core diameter due to the larger θ_D value for this atomizer.

Further, sheet thickness values obtained from experiments and the modified viscous model proposed by Rizk and Lefebvre[30] are compared in Table 5. Similar trends are observed for the sheet thickness values obtained by theory and experiments with variations in the exit area and injection pressure. Some discrepancies are observed in the sheet thickness values which can be attributed to the fact that the divergent section of the injector nozzle is not considered in the model. However, the actual exit area has been used in the viscous model of Rizk and Lefebvre[30] for evaluating analytical sheet thickness, for different nozzle configurations D1–D5. The sheet thickness measured in the experiments are lower than those predicted by the model, implying that providing the divergent section improves the spray atomization process significantly.

Break-up length

Another important characteristic of a spray is the break-up length of liquid sheet. Early break-up is

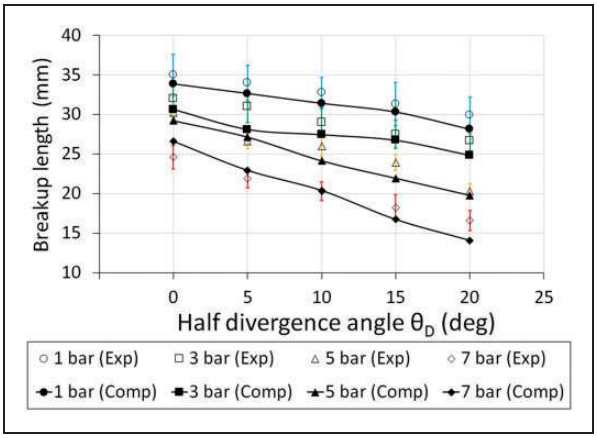

Figure 20. Break-up length for different atomizers at different injection pressures (comp – computational; exp – experimental).

desirable for improving the spray characteristics in the combustor. The break-up length of the liquid sheet emanating from the orifice continuously oscillates between two extreme values because of the flow unsteadiness and surface waves present. Thus, instantaneous images are used to measure the break-up length computationally as shown in Figure 9. Instantaneous values of break-up length are averaged to get the average break-up length for a given operating condition. The break-up length is measured on the basis of two conditions; either the sheet thickness decreases to 5% of the initial thickness at the orifice exit or the occurrence of a large gap with a size comparable to the maximum droplet size expected under the prevailing conditions. Several images are captured at different time instants using high-speed camera and are processed to obtain break-up length values experimentally. The ranges of experimental break-up length values for the five atomizers operated at four different pressures are plotted in Figure 20. The time-averaged break-up lengths predicted by computational analysis are also plotted for the sake of comparison.

In general, a good match is observed between the experimental and predicted break-up length data shown in Figure 20. The break-up length is found to be decreasing with increase in θ_D; since θ_D promotes a larger air core formation and thinner liquid sheet, it is not surprising that break-up length decreases with θ_D. The presence of a flowing air stream on both sides of the liquid sheet can induce shear instabilities within liquid sheet, which will aid in earlier break-up. At higher pressure, sheet breaks up earlier because of the increase in liquid velocity (higher Weber number). The computationally predicted break-up length has a maximum deviation of 14% from the corresponding experimental data.

Sauter mean diameter

Sauter mean diameter is another important parameter to characterize a spray. A PDI system is used to measure drop sizes at different axial and radial locations. SMD is plotted at the axial locations of 90, 120, and 150 mm downstream of the orifice. The line average SMD is calculated by using the drop size data at different radial locations at a particular axial location, across the diameter of the hollow cone spray. The spray cone angle, break-up length, and line average SMD are compared for different atomizers at the injection pressures of 3 bar and 7 bar in Tables 6 and 7, respectively. Despite the different trends observed for spray cone angle values, line-averaged SMD at all the axial locations (90, 120, and 150 mm) are found to be monotonously decreasing with increase in orifice divergence angle. This might be because of the strong interaction of the air phase with liquid phase inside as well as outside the atomizer.

Table 6. Experimentally measured spray cone angle, break-up length and SMD for different atomizers at different axial locations (injection pressure = 3 bar).

	Spray cone angle	Break-up length	Sauter mean diameter (μm)		
Atomizers	(deg)	(mm)	$x = 90$	$x = 120$	$x = 150$
D1	21.09	27.12	83.2	75.3	68.3
D2	23.97	25.9	81.2	76.2	64.3
D3	27.5	24.03	81.7	72.8	61.9
D4	28.05	22.5	75.6	66.1	58.1
D5	32.14	21.7	72.3	63.9	50.7

Table 7. Experimentally measured spray cone angle, break-up length, and SMD for different atomizers at different axial locations (injection pressure = 7 bar).

	Spray cone angle	Break-up length	Sauter mean diameter (μm)		
Atomizers	(deg)	(mm)	$x = 90$	$x = 120$	$x = 150$
D1	39.1	19.62	63.2	54.6	48.2
D2	33.07	16.94	65.3	57.8	49.6
D3	32.31	15.3	69.1	59.1	49.7
D4	34.79	13.24	62.5	55.2	45.4
D5	37.12	11.59	57.7	49.3	42.8

Conclusions

An experimental study has been carried out on the evolution of a liquid sheet, emanating from a pressure swirl atomizer with a diverging exit section. Two-phase flow simulations based on the VOF method have also been performed for understanding the interactions between the liquid and air streams inside the atomizer geometry.

The results indicate that the liquid sheet opens out and admits reverse air flow into the atomizer at larger divergence angles, thereby giving rise to air cone or air core formation. Due to air cone or air core formation, the thickness of liquid sheet close to the orifice exit reduces significantly; this in turn, leads to the generation of fine droplets. In fact, the strength of the reverse air flow within the atomizer increases with the increase in the divergence angle and the returning of air flow pushes the liquid sheet outwards. As a consequence, the spray cone angle increases with the increase in the divergence angle. At low divergence angles, air cone or air core are not formed; the corresponding liquid sheet thickness, spray break-up length, and the average droplet size (SMD) turn out to be larger. Measurements of liquid sheet thickness at orifice exit and break-up length are in good agreement with the results predicted by VOF simulations. The computational simulations clearly bring out the interactions between the liquid film and air core flow within the injector geometry and satisfactorily explain the trends observed at different orifice divergence angles.

The use of atomizer D5 (half divergence angle: 20°) induces fairly high spray cone angle, lower breakup length and finer droplet sizes (SMD) and thus this configuration is found to be superior over the other atomizers.

Acknowledgements

The authors are thankful to national centre for combustion research and development (NCCRD) for providing high-speed camera, double-pulsed Nd:YAG laser and phase Doppler interferometry (PDI) to perform the experiments.

Declaration of Conflicting Interests

The author(s) declared no potential conflicts of interest with respect to the research, authorship, and/or publication of this article.

Funding

The author(s) received no financial support for the research, authorship, and/or publication of this article.

ORCID iD

Kushal Ghate http://orcid.org/0000-0002-9702-8821
Thirumalachari Sundararajan http://orcid.org/0000-0001-9961-355X

References

1. Lefebvre AH and McDonell VG. *Atomization and sprays*. Boca Raton, FL: CRC Press, 2017.
2. Vijay GA, Moorthi NS and Manivannan A. Internal and external flow characteristics of swirl atomizers: a review. *Atom Sprays* 2015; 25: 153–188.
3. Ballester J and Dopazo C. Discharge coefficient and spray angle measurements for small pressure-swirl nozzles. *Atom Sprays* 1994; 4: 351–367.
4. Chu CC, Chou SF, Lin HI, et al. An experimental investigation of swirl atomizer sprays. *Heat Mass Transfer* 2008; 45: 11–22.
5. Lee EJ, Oh SY, Kim HY, et al. Measuring air core characteristics of a pressure-swirl atomizer via a transparent acrylic nozzle at various Reynolds numbers. *Exp Therm Fluid Sci* 2010; 34: 1475–1483.
6. Durdina L, Jedelsky J and Jicha M. Investigation and comparison of spray characteristics of pressure-swirl atomizers for a small-sized aircraft turbine engine. *Int J Heat Mass Transfer* 2014; 78: 892–900.
7. Landwehr F, Feggeler D, Walzel P, et al. A fibre sensor based frequency analysis of surface waves at hollow cone nozzles. *Exp Fluids* 2006; 40: 523–532.
8. Fu QF, Yang LJ and Qu YY. Measurement of annular liquid film thickness in an open-end swirl injector. *Aerosp Sci Technol* 2011; 15: 117–124.
9. Fu QF, Yang LJ, Zhang W, et al. Spray characteristics of an open-end swirl injector. *Atomiz Sprays* 2012; 22: 431–445.
10. Kim D, Kim S, Han P, et al. Effect of recess on mixing and atomization characteristics of liquid-liquid swirl coaxial injectors. *Atom Sprays* 2010; 20: 41–55.
11. Kim S, Khil T, Kim D, et al. Effect of geometric parameters on the liquid film thickness and air core formation in a swirl injector. *Meas Sci Technol* 2008; 20: 015403.
12. Schubring D, Ashwood AC, Shedd TA, et al. Planar laser-induced fluorescence (PLIF) measurements of liquid film thickness in annular flow. Part I: methods and data. *Int J Multiphase Flow* 2010; 36: 815–824.
13. Kang Y, Lin Y, Wang X, et al. Effects of sleeve divergence angle of dual-stage swirl cup on the ignition performance. In: *ASME turbo expo 2014: turbine technical conference and exposition*, 16 June 2014, pp.V04AT04A049–V04AT04A049. New York: American Society of Mechanical Engineers.
14. Radke CD, Meyer TR and Heindel T. Effect of injector exit geometry on atomization of a liquid-liquid double swirl coaxial injector using non-invasive laser. In: *50th AIAA/ASME/SAE/ASEE joint propulsion conference on optical and x-ray techniques*, 2014, p. 3787.
15. Halder MR, Dash SK and Som SK. Initiation of air core in a simplex nozzle and the effects of operating and geometrical parameters on its shape and size. *Exp Therm Fluid Sci* 2002; 26: 871–878.
16. Moon S, Abo-Serie E and Bae C. Air flow and pressure inside a pressure-swirl spray and their effects on spray development. *Exp Therm Fluid Sci* 2009; 33: 222–231.
17. Xue J, Jog MA, Jeng SM, et al. Influence of geometry on the performance of simplex nozzles under constant pressure drop. In: *Proceedings of the 15th annual conference on liquid atomization and spray systems*, Madison, WI, USA, May 2002.
18. Ma Z. *Investigation on the internal flow characteristics of pressure-swirl atomizers*. PhD Thesis, University of Cincinnati, USA, 2002.
19. Muthuselvan G, Ghate KD, Rao MS, et al. Experimental study of spray breakup phenomena in small-scale simplex atomizers with and without air swirl. *Atom Sprays* 2018; 28: 299–321.
20. Von Lavante E and Maatje U. Investigation of unsteady effects in pressure swirl atomizers. *ZARAGOZA* 2002; 9: 11.
21. Datta A and Som SK. Numerical prediction of air core diameter, coefficient of discharge and spray cone angle

of a swirl spray pressure nozzle. *Int J Heat Fluid Flow* 2000; 21: 412–419.
22. Yeh CL. Numerical investigation of liquid jet emanating from plain-orifice atomizers with chamfered or rounded orifice inlets. *JSME Int J Ser B* 2004; 47: 37–47.
23. Nouri-Borujerdi A and Kebriaee A. Numerical simulation of laminar and turbulent two-phase flow in pressure-swirl atomizers. *AIAA J* 2012; 50: 2091–2101.
24. Amini G. Liquid flow in a simplex swirl nozzle. *Int J Multiphase Flow* 2016; 79: 225–235.
25. Xue J, Jog MA, Jeng SM, et al. Effect of geometric parameters on simplex atomizer performance. *AIAA J* 2004; 42: 2408–2415.
26. Liu J, Zhang XQ, Li QL, et al. Effect of geometric parameters on the spray cone angle in the pressure swirl injector. *J Aerosp Eng* 2013; 227: 342–353.
27. Musemic E and Walzel P. Swirl atomizers with Coanda deflection outlets. In: *12th triennial international conference on liquid atomization and spray systems, ICLASS 2012*, Heidelberg, Germany, 2–6 September 2012.
28. Youngs and David L. Time-dependent multi-material flow with large fluid distortion. In: Mortom KW and Baines MJ (eds) *Numerical methods for fluid dynamics*. London: Academic Press, 1982, pp.273–486.
29. Issa RI. Solution of implicitly discretized fluid flow equations by operator splitting. *J Comput Phys* 1986; 62: 40–65.
30. Rizk NK and Lefebvre AH. Internal flow characteristics of simplex swirl atomizers. *J Propul Power* 1985; 1: 193–199.

Appendix

Notation

A_0	orifice area (m^2)
A_P	tangential port area (mm^2)
C_D	coefficient of discharge
D_0	orifice diameter (mm)
D_i	diameter of droplets in the i^{th} range (μm)
D_P	tangential port diameter (mm)
D_S	swirl chamber diameter (mm)
N_i	number of droplets in the i^{th} range (μm)
N_P	number of tangential ports
$\dot{m}_a$	actual mass flow rate (kg/s)
Q	volumetric flow rate (m^3/s)
r_t	orifice throat radius (μm)
SMD	Sauter mean diameter (μm)
t	liquid sheet thickness (μm)
t^*	normalized liquid sheet thickness
$\bar{U}$	average axial velocity component (m/s)
$\bar{W}$	average swirl velocity component (m/s)
V_{inlet}	radial velocity component at inlet (m/s)
W	annular inlet width (mm)
W_{inlet}	tangential velocity component (m/s)
ΔP	pressure differential across atomizer (bar, N/m^2)
ρ_l	liquid density (kg/m^3)
θ	spray cone angle (deg)
θ_D	half divergence angle (deg)